Soft X-ray radiation-damage studies in PMMA using a cryo-STXM

Tobias Beetz* and Chris Jacobsen

Department of Physics and Astronomy, SUNY Stony Brook, Stony Brook, NY 11794-3800, USA.
E-mail: tobias.beetz@stonybrook.edu

Radiation damage sets a fundamental limit for studies with ionizing radiation; cryo-methods are known to ease these limits. Here, measurements on mass loss and the decrease in the C═O bond density as measured by oxygen-edge XANES (NEXAFS) spectroscopy in thin films of poly(methylmethacrylate) (PMMA), studied in a vacuum, are reported. While cryo-methods allow more than 95% of the mass to remain at doses up to 10^7 Gy, there is little difference in C═O bond density *versus* dose between 298 K and 113 K sample temperatures. At both temperatures the critical dose for bond breaking is $\sim 15 \times 10^6$ Gy.

Keywords: soft X-rays; radiation damage; PMMA; XANES; STXM.

1. Introduction

Radiation damage is a limiting factor in imaging at high resolution with ionizing radiation. Basic considerations of image contrast indicate that doses of $\sim 10^6$ Gy are involved in 50 nm resolution imaging with soft X-rays (Sayre *et al.*, 1977; Gölz, 1992). These doses are sufficient to cause immediate changes in living cells, and to produce noticeable mass loss and shrinkage in some specimens that are wet but chemically fixed (Williams *et al.*, 1993). It is well known that cryo-methods can greatly reduce radiation damage in biological specimens (Glaeser & Taylor, 1978; Dubochet *et al.*, 1987). Cryo-X-ray microscopy experiments at 113 K have shown essentially no observable mass loss at the 50 nm spatial resolution level with radiation doses up to $\sim 10^{10}$ Gy (Schneider, 1998; Maser *et al.*, 2000). However, mass loss is not the only mechanism of radiation damage, and cryo-methods are found to improve but not eliminate degradation of high-resolution electron diffraction data (Glaeser & Taylor, 1978). Overall mass density can be preserved while chemical bonds are not preserved. This suggests that cryo-methods may offer differing degrees of protection for spectroscopy, atomic-resolution imaging or diffraction than simple mass-loss measurements would suggest.

Radiation-damage effects in soft X-ray spectroscopy have been studied by measuring the loss of X-ray absorption near-edge structure (XANES) spectroscopic resonances in thin organic films. Zhang *et al.* (1995) used carbon XANES to monitor the decrease in C═O bond density due to chain scission, and the increase in C═C bond density due to crosslinking, in room-temperature PMMA films that were first baked at various temperatures. The C═O bond density was found to decrease exponentially with increasing dose, with a characteristic dose of $\sim 13 \times 10^6$ Gy. Coffey *et al.* (2002) studied several other thin polymer films with carbon XANES, and investigated the influence of atmospheric oxygen on the radiation-damage chemistry. These authors found that the damage rate in a helium atmosphere is slowed down by a factor of approximately 100 relative to air for their poly-(ethylenetherephthalate) (PET) sample. Their experiments were also conducted at room temperature. These studies provide the background to our goal of examining radiation damage using XANES spectroscopy for samples at cryogenic and room temperatures.

2. Materials and methods

2.1. PMMA sample

A PMMA film prepared on top of a silicon nitride window served as our sample. The silicon nitride window was produced by back-etching silicon from a wafer with a nitride layer grown on it, resulting in 100 nm-thick silicon nitride windows. The PMMA (MW 950 KD PMMA C6 from MicroChem) was spun onto the window at 7000 r.p.m. from a solution 6% by weight in chlorobenzene. We note here that the high molecular weight of the PMMA used should not affect the relative molecular weight reduction since the G-factor is largely independent of the molecular weight (Dawes & Glover, 1996; Smith *et al.*, 2001). The PMMA samples were baked at 423 ± 1 K for 2 h. The thickness of the PMMA layer was then measured using a Tencor Instruments Alpha-Step 200 profiler to be 580 ± 20 nm. The chemical structure of PMMA is shown in Fig. 1.

The carbonyl functional group gives rise to a peak in the oxygen XANES spectra at 531.5 eV (Fig. 3) which is due to the O $1s$(C═O) $\rightarrow \pi^*_{C=O}$ transition (Tinone *et al.*, 1994). The decrease in intensity of this transition with increasing dose is used later to quantify the damaging effects.

2.2. Experimental description

The data presented here were acquired using the Stony Brook cryo-scanning transmission X-ray microscope (cryo-STXM) (Maser *et al.*, 2000), which is part of the X1A undulator beamline at the National Synchrotron Light Source (Winn *et al.*, 2000). The imaging mode of the cryo-STXM was used to deliver a known dose to the specimen. This was achieved by scanning the specimen with a step size of 40 nm through the focal spot provided by a Fresnel zone plate with a diameter of 160 μm, a central stop diameter of 80 μm and 45 nm outermost zone width. A phosphor-coated photomultiplier tube with 6.6% detection efficiency at 525 eV (see §2.2.3) recorded the transmitted flux at each step. A typical focused flux during exposure was approximately 1.8 MHz, resulting in 1.1 MHz after transmission through the PMMA sample. The incident flux of 1.8 MHz corresponds to a flux density of ~ 7 photons s^{-1} nm^{-2} averaged over the central Airy disc of the zone-plate's point spread function. The exposure at liquid-nitrogen temperature was carried out using a 10 ms pixel dwell time whereas the room-temperature exposure was carried out using a 5 ms pixel dwell time. With the energy of the damaging X-rays tuned to 525.0 eV, the dose during such a scan was approximately 7.0×10^6 Gy at liquid-nitrogen temperature and approximately 3.7×10^6 Gy at room temperature (see §2.3 for details). After the dose scan, the spectroscopy mode of the cryo-STXM was used to record an oxygen XANES spectrum across the oxygen *K*-edge. Since radiation dose is defined as energy

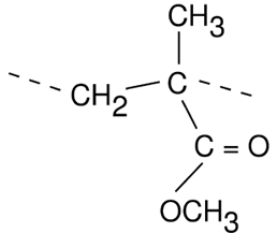

Figure 1
Chemical structure of PMMA.

absorbed per mass, which in turn is proportional to the exposed area, the beam was defocused to ~3.6 μm during spectrum scans to produce a dose of only $\sim 0.6 \times 10^6$ Gy per scan.† The same absorbed energy was therefore put into a larger area, allowing for low-dose spectroscopy. The sequence of dose scan and spectroscopy scan was then repeated about 20 times to give a cumulative dose to the specimen of more than 10^8 Gy. Finally, an in-focus image with a lower dwell time and a larger step size over a larger field was taken to ensure that the specimen remained centred on the X-ray beam axis. Fig. 2 shows such images of dosed regions at both recording temperatures.

To normalize the recorded spectra, a spectrum of an area with no PMMA on the window was recorded at the beginning of each sequence and used as an I_0 spectrum.

2.2.1. Sample conditions. The cryo-STXM with its vacuum chamber was designed to handle specimens cooled to liquid-nitrogen temperature. In the first set of experiments the PMMA sample was cooled down to liquid-nitrogen temperature prior to exposure. The sample was then allowed to warm up to room temperature, before Fig. 2(*c*) was acquired. The second experiment was conducted with the PMMA sample at room temperature.

2.2.2. Energy calibration. To calibrate the energy of the oxygen XANES spectra, we added O_2 gas into the path of the X-ray beam. The strong absorption at 530.82 eV (Hitchcock, 1994) was then used to calibrate the spectra.

2.2.3. Detector calibration. Knowledge of the efficiency of the phosphor-coated photomultiplier detector is important for calculating the exact dose delivered to the sample. This was determined by comparing the count rate on the detector of a collimated beam of focused X-rays with the current measured on a photodiode that has an almost 100% efficiency (Funsten *et al.*, 1997). The measured detector efficiency was about 6.6% at 525 eV.

2.3. Dose calculations

The skin dose (dose deposited in the surface layer of an absorber) can be calculated using the 1/*e* absorption length as

$$\text{Dose} = 1.602 \times 10^{-4}(ENt\mu/\rho A\eta)\ \text{Gy}, \qquad (1)$$

where E is the photon energy in eV, N is the number of photons per second absorbed by the sample, measured in kHz, η is the efficiency of the detector, t is the exposure time in ms, ρ is the density in g cm^{-3}, A is the radiated area in μm^2, d is the thickness and μ is the inverse absorption length in μm^{-1}.

The 1/*e* absorption length can be expressed as

$$1/\mu = 2r_e\lambda(N_A/A)\rho f_2,$$

where $r_e = 2.812 \times 10^{-15}$ m, N_A is Avogadro's number, A is the atomic weight and f_2 is the imaginary part of the complex atomic scattering factor, which can be found from tabulated values (Henke *et al.*, 1993). This gave, for example, an assumed absorption length for PMMA of $1/\mu = 1.1$ μm at 525.0 eV. A typical dose during an exposure was approximately 7.0×10^6 Gy for an exposure at liquid-nitrogen temperature and approximately 3.7×10^6 Gy for an exposure at room temperature. During a spectral scan, a typical dose was $\sim 0.6 \times 10^6$ Gy. Note that the dose in a spectral scan is still a high dose even though we widened the X-ray beam to a diameter of ~3.6 μm and used a short dwell time. The short dwell time is also the reason for the relatively low signal-to-noise ratio in the spectral scan.

2.4. Fitting the spectra

The absorption peak due to the C═O bond density was fitted with a Gaussian. The height of the Gaussian was later used to quantify the loss of the C═O bond density under radiation. We note here that although XANES spectra were recorded at doses exceeding 10^8 Gy we only used data up to $\sim 35 \times 10^6$ Gy for our analysis, since the fit of the C═O bond peak for higher doses could not be made with a high level of certainty.

To determine the mass loss, each spectrum was fitted with an average value at the low-energy (528.0–529.5 eV) and at the high-energy (538.5–540.0 eV) end of the spectrum (Fig. 3). The ratio of the two average values was used to determine the oxygen mass loss as a function of dose using differential absorption analysis (Engström, 1946).

3. Results and discussion

3.1. Spectroscopic observations

To quantify the loss of the carbonyl group, the heights of the C═O absorption peaks determined from the XANES spectra are plotted *versus* the dose in Fig. 4. The data were fitted according to

$$\text{BD} = \text{BD}_\infty + A\exp(-a/a_c), \qquad (2)$$

where a is the radiation dose, a_c is called the critical dose for the loss of the C═O bond density and BD_∞ is the remaining C═O bond density after infinite radiation dose. The figure shows both curves for the PMMA sample at liquid-nitrogen and room temperatures. Table 1 summarizes the fitting coefficients obtained.

From the decay rate of the C═O bond density at both temperatures it can be concluded that the specimen temperature has no influence on preserving XANES signatures of the chemical state of the specimen, at least in this example system.

3.2. Mass loss

The dependence of mass loss on dose is shown in Fig. 4 for both temperatures. Following Coffey *et al.* (2002), the mass loss (or loss in optical density) can be quantified by

$$\text{OD} = \text{OD}_\infty + B\exp(-b/b_c), \qquad (3)$$

where b is the radiation dose, b_c is called the critical dose and OD_∞ is the remaining optical density after infinite radiation dose. The fitting coefficients are also summarized in Table 1. We note here that, for a confident value of OD_∞ at liquid-nitrogen temperature, more data at

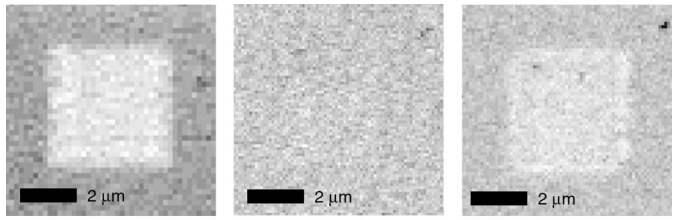

(*a*) (*b*) (*c*)

Figure 2
(*a*) Coarse area scan at room temperature of a region that was dosed at room temperature. The square in the middle indicates the mass loss of the dosed region. (*b*) Coarse area scan at liquid-nitrogen temperature of the region that was dosed at liquid-nitrogen temperature. The image shows no visible mass loss at the dosed region. (*c*) Same area as that in image (*b*) but after warming up the sample; the dosed region becomes visible.

† During a spectrum scan the widened beam will drift slightly off the previously radiated area as we scan to higher energies. From alignment measurements we calculate that drift-off effects become important above 534 eV and reach a maximum at an energy of 540 eV, where 10% of the incident photons will be off the radiated area, corresponding to a systematic error of 0.1 in terms of the optical density.

higher radiation doses would have to be collected. However, since the focus of this report is on spectroscopic limits, we did not investigate higher radiation doses.

Our critical dose of $\sim 18 \times 10^6$ Gy at 525.0 eV for the control experiment at room temperature is in good agreement with the previously obtained value of 13×10^6 Gy at 317 eV by Zhang *et al.* (1995) and 14×10^6 Gy at 315 eV by Coffey *et al.* (2002). The higher dose that we obtained in our measurements may be explained in part by the fact that an additional dose of $\sim 0.6 \times 10^6$ Gy was estimated to be applied while acquiring a spectral scan. As we have seen in §2.3, the dose during a spectral scan is relatively high even though the beam was defocused. A better quantitative measurement of the dose should therefore include more exact information on the dose delivered during such a spectral scan. We also note that the difference may be due to the fact that a different weighting of molecular dissociations is obtained at 525.0 eV than at 315 or 317 eV, respectively.

4. Conclusions

We have shown that the C═O bond in irradiated PMMA is broken at comparable rates at liquid-nitrogen and room temperatures. We have confirmed that cryogenic sample conditions are extremely effective for reducing mass loss, as is required for non-atomic-resolution imaging applications such as nanotomography (Wang *et al.*, 2000; Weiss *et al.*, 2000). However, cryogenic sample conditions do not have a measurable affect on the soft X-ray radiation dose sensitivity of chemical bonds, at least in this model case of XANES spectroscopy of PMMA with no water present. We note that PMMA is much more sensitive to radiation damage than many other polymers, and that there also may be significantly different mechanisms (such as free-radical formation) acting in the case of hydrated organic molecules. Further experiments to study radiation-damage effects on hydrated protein solutions are in preparation.

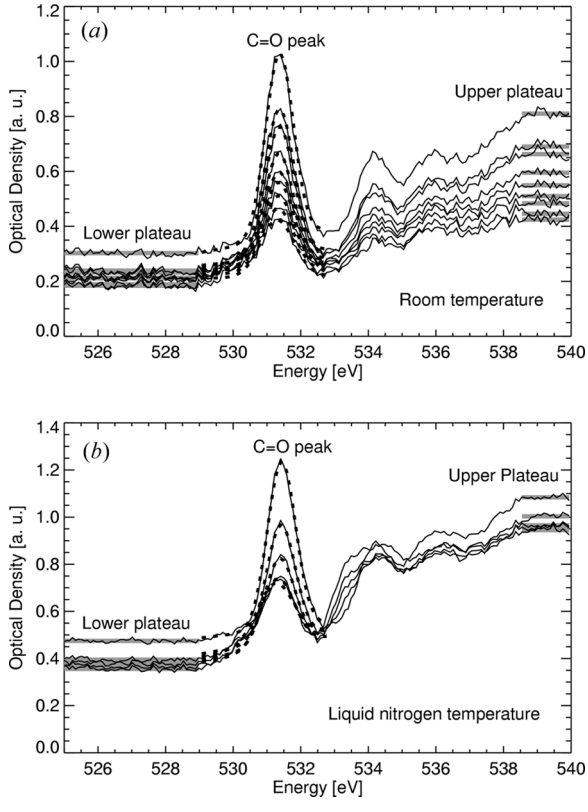

Figure 3
Oxygen XANES spectra of PMMA, showing the dependence on the dose at (*a*) room temperature and (*b*) liquid-nitrogen temperature. The spectra show the decrease of the C═O bond density with increasing dose. The C═O bond peaks were fitted using Gaussians. Also shown are the average values, denoted by upper and lower plateaus, used to determine the oxygen mass loss.

Table 1
Fit coefficients for loss of C═O bond density and mass loss according to equations (2) and (3).

The data and the actual fit are shown in Fig. 4. The critical dose values are given in units of 10^6 Gy. The remaining optical density at 113 K is uncertain owing to the limited range of radiation doses that were probed in this experiment.

	C═O loss			Mass loss		
	A	a_c	BD_∞	B	b_c	OD_∞
298 K	0.81	18	0.18	0.89	34.8	0.12
113 K	0.73	13	0.18	0.89	597	(0.11)

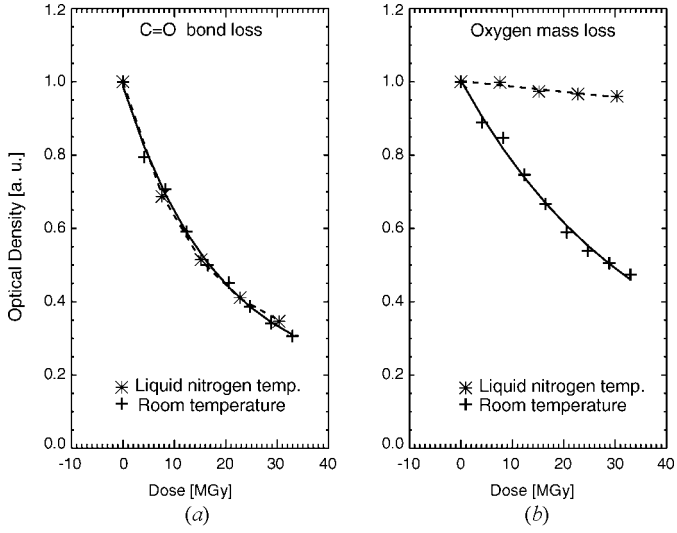

Figure 4
(*a*) Loss of C═O peak intensity and (*b*) mass loss as a function of dose at liquid-nitrogen and room temperatures. The data were fitted using equations (2) and (3), where the fitting coefficients are summarized in Table 1.

We thank Jaan Mannik for the PMMA sample preparation, and Michael Feser, Sue Wirick and Barry Winn for great help with the cryo-STXM and for stimulating discussions. This research was carried out at the National Synchrotron Light Source, Brookhaven National Laboratory, and was supported by the NSF under grants ECS-0099893 and DBI-9986819.

References

Coffey, T., Urquhart, S. G. & Ade, H. (2002). *J. Electron Spectrosc. Relat. Phenom.* **122**, 65–78.
Dawes, K. & Glover, L. C. (1996). *Physical Properties of Polymers Handbook*, edited by J. E. Mark, ch. 41, pp. 557–576. New York: AIP Press.
Dubochet, J., Adrian, M., Chang, J. J., Lepault, J. & McDowall, A. W. (1987). *Cryotechniques in Biological Electron Microscopy*, edited by R. A. Steinbrecht & K. Zierold, pp. 114–131. Berlin: Springer-Verlag.
Engström, A. (1946). *Acta Radiol. Suppl.* **63**, 1–106.
Funsten, H. O., Suszcynsky, D. M., Ritzau, S. M. & Korde, R. (1997). *IEEE Trans. Nucl. Sci.* **44**, 2561–2565.
Glaeser, R. M. & Taylor, K. A. (1978). *J. Microsc.* **112**, 127–138.

Gölz, P. (1992). *X-ray Microscopy III*, edited by A. G. Michette, G. R. Morrison & C. J. Buckley, *Springer Series in Optical Sciences*, Vol. 67, pp. 313–315. Berlin: Springer-Verlag.
Henke, B. L., Gullikson, E. M. & Davis, J. C. (1993). *Atom. Data Nucl. Data Tables*, **54**, 181–342.
Hitchcock, A. P. (1994). *J. Electron Spectrosc. Relat. Phenom.* **67**, 1–132.
Maser, J., Osanna, A., Wang, Y., Jacobsen, C., Kirz, J., Spector, S., Winn, B. & Tennant, D. (2000). *J. Microsc.* **197**, 68–79.
Sayre, D., Kirz, J., Feder, R., Kim, D. M. & Spiller, E. (1977). *Ultramicroscopy*, **2**, 337–341.
Schneider, G. (1998). *Ultramicroscopy*, **75**, 85–104.
Smith, A. P., Spontak, R. J. & Ade, H. (2001). *Polym. Degrad. Stab.* **72**, 519–524.
Tinone, M. C. K., Tanaka, K., Maruyama, J., Ueno, N., Imamura, M. & Matsubayashi, N. (1994). *J. Chem. Phys.* **100**, 5988–5995.
Wang, Y., Jacobsen, C., Maser, J. & Osanna, A. (2000). *J. Microsc.* **197**, 80–93.
Weiss, D., Schneider, G., Niemann, B., Guttmann, P., Rudolph, D. & Schmahl, G. (2000). *Ultramicroscopy*, **84**, 185–197.
Williams, S., Zhang, X., Jacobsen, C., Kirz, J., Lindaas, S., van't Hof, J. & Lamm, S. S. (1993). *J. Microsc.* **170**, 155–165.
Winn, B., Ade, H., Buckley, C., Feser, M., Howells, M., Hulbert, S., Jacobsen, C., Kaznacheyev, K., Kirz, J., Osanna, A., Maser, J., McNulty, I., Miao, J., Oversluizen, T., Spector, S., Sullivan, B., Wang, S., Wirick, S. & Zhang, H. (2000). *J. Synchrotron Rad.* **7**, 395–404.
Zhang, X., Jacobsen, C., Lindaas, S. & Williams, S. (1995). *J. Vac. Sci. Technol.* B**13**, 1477–1483.

 Received 5 July 2002 • Accepted 7 February 2003